PERFORMANCE OF RC WALL BUILDING SUBJECTED TO EARTHQUAKE AND TSUNAMI IN SEQUENCE

S.J. Tagle[1], R. Jünemann[2], J. Vásquez[3], J.C. Llera[4], M. Baiguera[5]

[1] *Graduated Master student, Department of Structural and Geotechnical Engineering Pontifical University of Chile, sotagle@uc.cl*

[2] *Professor, Department of Structural and Geotechnical Engineering Pontifical University of Chile, rjunemann@ing.puc.cl*

[3] *Investigator, National Research Center of Integrated Natural Disaster Management (CIGIDEN), jorge.vasquez@cigiden.cl*

[4] *Professor, Department of Structural and Geotechnical Engineering Pontifical University of Chile, jcllera@ing.puc.cl*

[5] *Research Fellow, Civil Environmental and Geomatic Engineering Department University College London, m.baiguera@ucl.ac.uk*

Abstract

Chile is in one of the most seismically active areas in the world and due to its location and geography, strong ground motions are usually followed by large tsunamis. Thus, high density coastal cities in Chile are exposed not only to earthquakes but also to tsunamis. Typically, residential buildings in Chile are medium-rise reinforced concrete (RC) wall buildings, which have shown adequate seismic behavior in the strong events of the last decade in terms of preventing collapse and protecting human life. Additionally, these buildings have shown adequate behavior after the latest tsunamis following the 2010 Maule earthquake and 2015 Illapel earthquake, were only non-structural damage was observed in first stories due to the tsunami action. Although there is a significant exposure of RC wall buildings to the sequential action of earthquake and tsunami, most of the research has been focused mainly on the seismic behavior of these structures. Little research has been found regarding the tsunami behavior of this type of buildings, and even less regarding the sequential action of both earthquake and tsunami. In order to understand the behavior of the typical Chilean residential buildings to both hazards, a real building is selected as a case study. Nonlinear finite element simulations of a representative slice of the building are performed using the software DIANA considering a double pushover analysis. The earthquake pushover is applied first until a specific damage state is reached and then the earthquake loading is removed. Then, the tsunami pushover is applied considering only the hydrodynamic forces of the wave through the variable depth pushover (VDPO) approach. Additional effects such as flooding at the back of the building, buoyancy, uplift and debris impact were neglected. A set of tsunami load cases are evaluated considering different loading directions and Froude numbers. Based on the results of this research, the main variables affecting the tsunami capacity of the building are analyzed, and the impact of the previous earthquake damage in the tsunami capacity of the building is discussed.

Keywords: earthquake and tsunami in sequence; shear wall damage; reinforced concrete building

1. Introduction

Tsunamis have caused significant human and economic losses in many countries around the world in the last decade. Some of the most significant cases are the 2004 Indian Ocean tsunami, and the 2011 tsunami off the Pacific coast of Japan. The 2004 Indian Ocean tsunami reached several different countries such as Indonesia, Thailand, Sri Lanka, India and other East African countries. These events caused widespread damage to cities, infrastructures and environment, along with the death of more than 150,000 people [1]. The 2011 tsunami in Great East Japan caused 19,000 deaths and around US$211 billion in direct losses [2].

In the case of Chile, strong ground motions are usually followed by large tsunamis [3]. Notably, the 1960 $M_w = 9.5$ Valdivia earthquake and the 2010 $M_w = 8.8$ Maule earthquake were followed by tsunamis that killed hundreds of people along the coast [3,4]. Moreover, inundation depths ran from a few meters to over 20 meters, causing significant damage to urban environments and infrastructures. The observed damage ranged from the complete destruction of cars and small houses, to the lifting and displacement of large objects such as boats and even buildings.

Tsunamis are massive waves triggered by a body of water after earthquakes, landslides or other disturbances. Once the wave or series of waves reach the shore at high speed, light structures are dragged by the flow while other systems are impacted by the flow causing significant hydrodynamic forces. In the case of earthquake-triggered tsunami, the inundation may impact a structure that has already undergone structural damage due to seismic action. Therefore, the question that motivates this research is to quantify the impact of the tsunami on a typical Chilean residential building that has already suffered damage in the preceding earthquake.

Most research on earthquake and tsunami behavior and the performance of structures has been focused on each action separately, but limited literature has been found on the sequential actions of earthquakes and tsunamis [5]. De la Barra [6] studied the behavior of a RC building subjected to seismic action followed by a tsunami using pushover analysis. In this study, a shear wall building constructed in 1979 and designed to the old Chilean design code was considered as a case study, and a resisting plane of the building was modeled using fiber elements in OpenSees. This research concluded that, independently from the previous damage caused by the earthquake, the system was able to sustain a tsunami net force greater than the earthquake, without experiencing a considerable reduction in its capacity to resist the tsunami. In addition, Latcharote [7] studied a RC building under the sequential action of earthquake and tsunami. A wall-frame model of a 7-story wall-frame building was developed and subjected to earthquake ground motion, followed by static pushover analysis with a uniform pressure to represent the tsunami load. The conclusion of this investigation is that more damage is observed after tsunami load, especially at the first-floor level.

This paper presents an investigation on the behavior of a typical Chilean RC shear wall building subjected to the sequential action of earthquake and tsunami via a double pushover analysis approach. The case study building is a medium rise RC wall building constructed in 2005 and located in Santiago, Chile. The building was damaged during the Maule earthquake and its seismic performance has previously been studied in detail [8,9]. Nonlinear finite element (FE) simulations of a fictitious slice of the building are performed using the software DIANA [10].

2. Inelastic Finite Element (FE) Model of a RC Wall

Nonlinear finite element simulations of RC walls are performed using the software DIANA 10.2 [10] since it has shown good results in previous research regarding RC wall behavior [8,9,11]. Inelastic constitutive models for concrete and steel are considered. The total strain rotating crack model is used to model concrete behavior, based on the Modified Compression Field Theory, proposed initially by Vecchio and Collins [12]. In this case, the parabolic model is considered to model compressive concrete behavior, while the Hordijk model [13] is considered for tensile behavior, both models are based on

2

fracture energy [10]. To model steel behavior, the Menegotto-Pinto model [14] is used. This constitutive model does not include bar buckling or fracture. The type of element used to model concrete elements is the Q20SH (DIANA [10]). This is a curved shell quadrilateral element with four nodes and four Gauss quadrature points [15]. This type of element has demonstrated good results in reproducing the expected behavior of RC walls [11] due to its ability to capture the out of plane buckling of the wall. The element used to model the reinforced steel is the "bar" element, which is an embedded element that assumes perfect bonding [10].

A real RC wall building, representative of a typical Chilean residential building, was selected as a case-study. The building under study has 18 floors, 2 basements and a typical story floor plan schematically shown in Fig.1. The thickness of all the walls and slabs is 20 cm and 15 cm, respectively.

This building suffered brittle failures in some RC walls after the Maule 2010 earthquake, particularly walls at axes U, Q and N, as shown in Fig.1a for wall Q. The damaged walls present an irregularity in height with a flag-shaped configuration, as shown in Fig.1c. The damage was typically concentrated within the basements in the wall irregularity. The crack propagated horizontally where concrete crushing and buckling of rebars was observed [8].
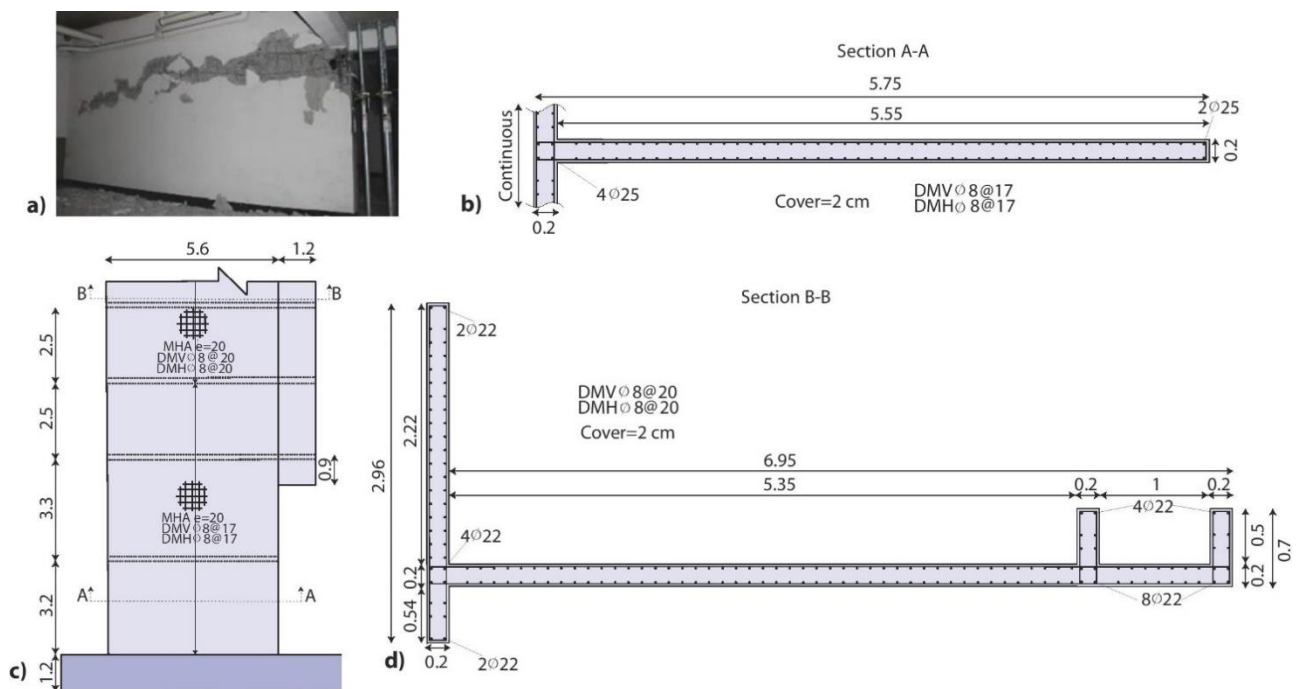

Fig. 1 – a) Wall at axis Q damaged after earthquake Jünemann et al [8]; b) Section A-A of wall at axis Q (dimensions in m); c) Structural specifications wall at axis Q (dimensions in m); d) Section B-B of wall at axis Q (dimensions in m)

A simplified model of the building is developed with the aim of reproducing the response of the building at a lower computational cost than the previously developed 3D inelastic models of the entire building [9]. The wall at axis Q (shown in red in Fig.2) is selected as a case study. This wall has a flag-shaped configuration, as shown in Fig.1c, and it has a cross section that varies along the height of the building (Fig.1b and 1d). In the basement, the flange goes along the entire width of the building. However, from the first floor upwards, the length of the flange is reduced to 2.96 m.
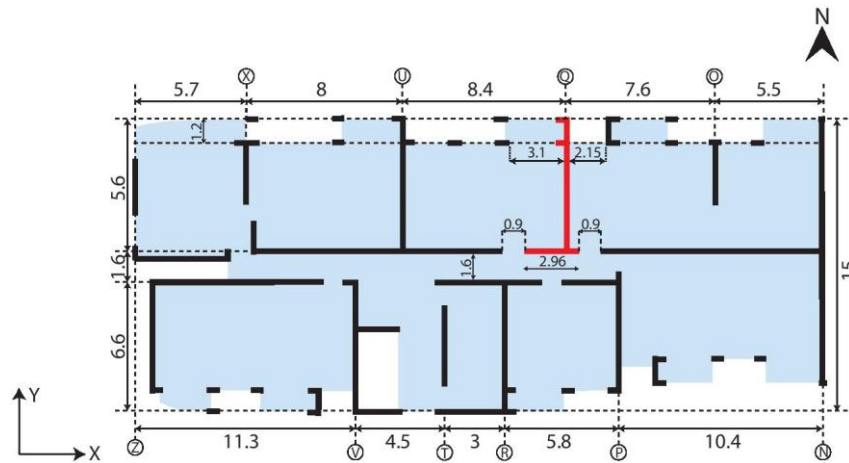
3

Fig. 2 – Typical story floor plan (dimensions in meters)

Previous studies have shown that considering only the isolated cantilever wall does not represent the expected behavior [8]. Thus, in order to capture the 3D interaction between the wall and the rest of the building, it is necessary to include a complementary portion of the building. Since the building is not exactly symmetrical (Fig.2), the selected wall is replicated in mirror form, as shown in Fig.3.

The wall separation Sw is taken as 1.6 m, which corresponds to the aisle width in the original project, while the slab width Ws is 3.8 m, which corresponds to the wall flange width on a typical story plus half of the door width (0.45 m) at each side of Q axis (Fig.2). Finally, the wall flange width at the basement Fbw is taken as 8 m, corresponding to half the distance of each wall located next to wall Q at the basement level. These variables were selected based on a sensitivity analysis developed elsewhere [16].

The nominal material properties specified in the design of the building are used in the model. A yield stress of 420 MPa is considered for steel, and concrete compressive strength of $f'_c = 25\ MPa$ is used. Only unconfined concrete is considered. For computational economy, nonlinear concrete and reinforcing steel rebars are considered only up to the 5th floor, and from 6th floor upwards only linear concrete is considered. The translation in X,Y and Z directions are restricted at the base nodes of both walls. Additionally, the translation in the X direction is restricted at the free borders of the slab. No rigid diaphragm is considered.
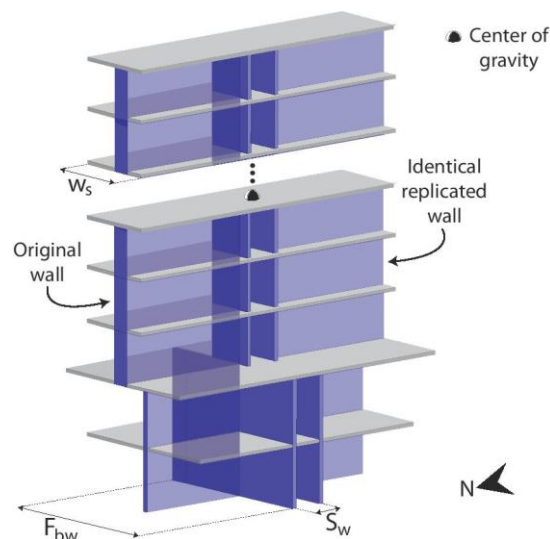

Fig. 3 – Simplified model and their variables

4

3. Earthquake loading

An earthquake pushover analysis is developed on the simplified model with load pattern of roof displacement until different damage states are reached. The pushover curve in terms of base shear versus roof displacement for each damage state and their schematic damage are shown in Fig.4a and 4b, respectively. Damage state I (D_I) corresponds to the first crack in tensioned concrete (point 1 in Fig.4b), which occurs at 2.7 roof displacement. Damage state II (D_{II}) corresponds to the yielding of reinforcing bars in compression (point 2 in Fig.4b), occurring at 10.3 cm of roof displacement. Damage state III (D_{III}) occurs when the peak strength of the structure is reached (point 3 in Fig.4b), which in this case occurs at 13.9 cm of roof displacement. Finally, Damage state IV (D_{IV}) corresponds to the final state after the occurrence of a brittle failure due to concrete crushing in the critical section (point 4 in Fig.4b).

In order to apply the earthquake and tsunami in sequence, the model is loaded up to a specific damage state, and then unloaded until zero base shear condition, which corresponds to the final state after earthquake loading, and the initial state for tsunami loading. Fig.4a shows the loading and unloading process of the earthquake pushover at the different damage states. For damage state D_I, the behavior of the structure is purely elastic. The loading and unloading occurs through the same linear curve and there are no residual deformations after unloading. For damage states D_{II} and D_{III}, the loading and unloading does not occur along the same curve, the inelastic excursions are limited, and residual deformations are very small, as shown in the zoom in Fig.4a. For damage state D_{VI}, significant inelastic excursions occur, and residual deformations are significant in size (4.7 cm).

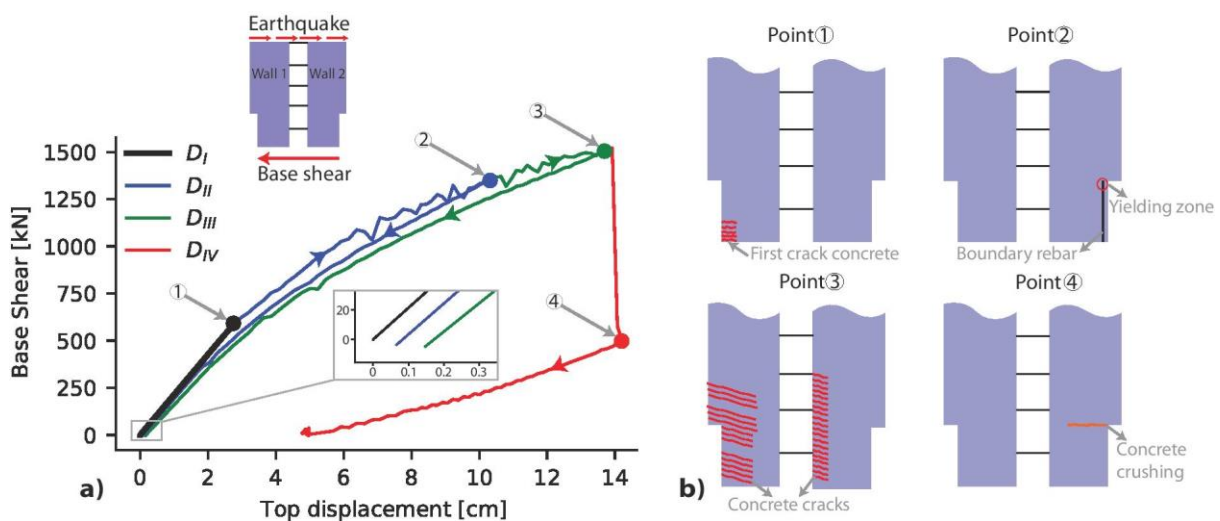

Fig. 4 – Earthquake pushover loading - unloading for different damage states; b) schematic damage for each damage state

4. Tsunami loading

In order to adequately represent the tsunami effect on the structure for assessment purposes, this research focuses on the variable depth pushover (VDPO), which correspond to a hydrodynamic loading approach proposed by Petrone et al. [5]. This study is based on the previous work by Qi et al. [17], which defines the tsunami hydrodynamic force acting on an obstacle. In this approach, a dense area of buildings is assumed and additional effects such as flooding at the back of the building, buoyancy, uplift and debris impact were neglected. The location of the tsunami load is presented in Fig.5.
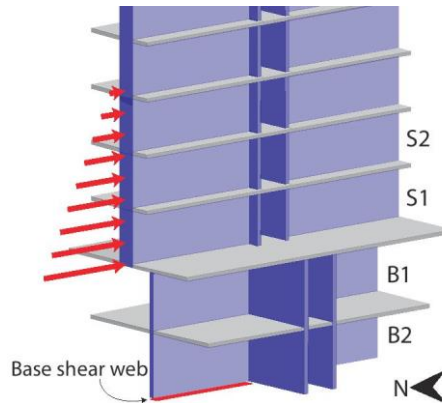
5

Fig. 5 – Location of tsunami load as nodal forces along the strong axis of the wall and location of base shear web

The tsunami net force (F), experimentally obtained by Qi et al [17], is presented in Eq. (1), where C_d is the drag coefficient; u is the flow velocity; g is the acceleration of gravity; ρ is the density of the fluid; h the wave height; λ is a leading coefficient; and b the tributary width where the tsunami is applied. $F_r = u/\sqrt{gh}$ is the Froude number and F_{rc} is the Froude number threshold [17]. For the VDPO, the Froude number is kept constant and the wave height is varied.

$$\frac{F}{b} = sign(u) \begin{cases} 0.5C_d\rho u^2 h & if\ F_r < F_{rc} \\ \lambda\rho g^{1/3}u^{4/3}h^{4/3} & if\ F_r \geq F_{rc} \end{cases} \tag{1}$$

The Froude number is a parameter depending on the tsunami depth and flow velocity, thus each tsunami event can be characterized by a specific Froude number. However, there is no recorded information on flow velocity from past tsunami events in Chile. Therefore, Froude numbers estimated by Asai et al. [18] in different locations after 2011 Great East Japan earthquake are used. The values considered for the Froude number in the present investigation are 0.6 and 1.27, which represent low and high Froude number limits for areas prone to tsunami inundation [18].

5. Earthquake and tsunami in sequence

A double pushover analysis of earthquake and tsunami in sequence is applied in this section to the simplified model. The schematic loading sequence is described in Fig.7, where three phases can be distinguished:

(i)   Earthquake pushover loading: seismic load is statically applied through lateral roof displacements *Δu* until a specific damage level is reached (Fig.7a).

(ii) Earthquake pushover unloading: lateral roof displacements - *Δu* are statically applied in the opposite direction until zero base shear is reached (Fig.7b).

(iii) Tsunami pushover loading: tsunami load is statically applied starting from the first floor, using the VDPO approach and considering the tributary area according to Fig.7c and 7d. The tsunami force can either positive, i.e. applied in the same direction as the earthquake (Fig.7c); or negative, i.e. in the opposite direction to the earthquake (Fig.7d). Additionally, two Froude number values are considered: F_r=0.6 and F_r =1.27.
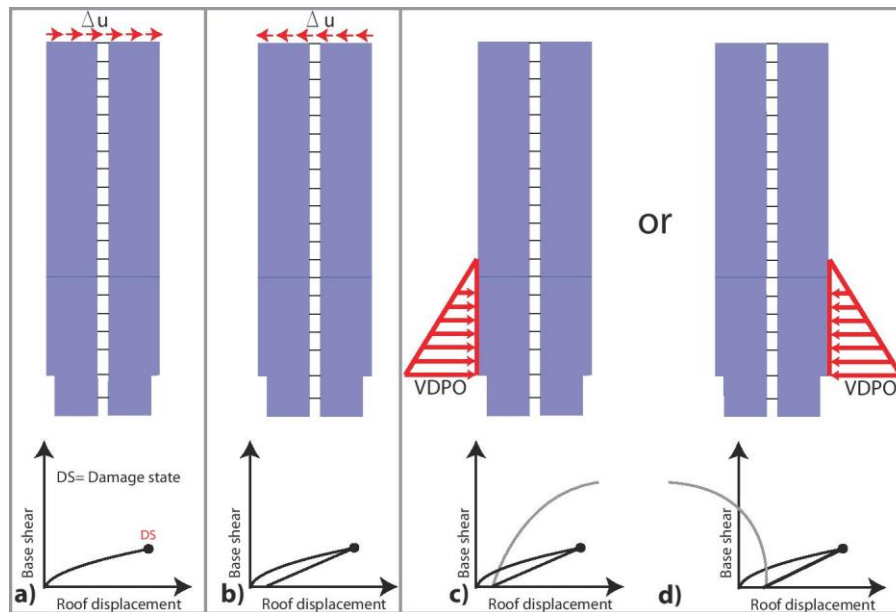
6

Fig. 7 – a) loading seismic pushover; b) unloading seismic pushover; c) loading positive tsunami.; and d) loading negative tsunami

First, a pure tsunami case is evaluated, i.e. only stage iii) is applied to the simplified model. This is a case without previous earthquake damage called D_0. In this case, the direction of the tsunami has no effect due to the symmetry of the simplified model. Fig.8 shows the results obtained for the tsunami pushover (positive or negative) for the case without previous damage (D_0) for Froude numbers $F_r=0.6$ and $F_r =1.27$. Results show that the behavior in terms of the pushover curve shape is similar for both Froude numbers, but the peak values are different. Regarding the base shear (Fig.8a), for $F_r =1.27$ higher base shear is obtained compared to $F_r =0.6$, while higher top displacement is observed in the latter case. Fig.8b shows a significant influence of the Froude number in the tsunami height. For $F_r =1.27$ the maximum tsunami height is 8.7 m, while for $F_r =0.6$ is 13.4 m.

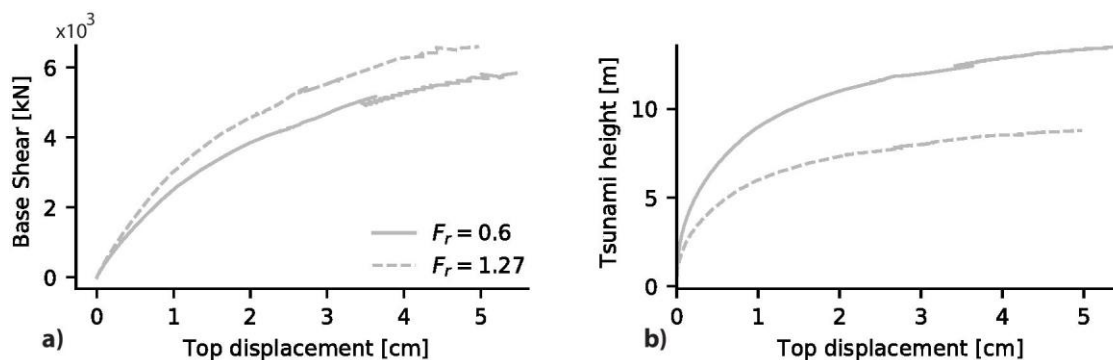

Fig. 8 – Tsunami pushover for the case without previous earthquake damage D_0: a) base shear versus top displacement; and b) tsunami height versus top displacement

Now, the double pushover analysis is applied considering the four damage states as previously defined in section 3, i.e., damage states D_I, D_{II}, D_{III} and D_{IV} are considered for the earthquake. Then, the tsunami is applied in the two directions (positive or negative), and taking into consideration the two Froude numbers ($F_r=0.6$ and $F_r =1.27$). Results are shown in Fig.9 in terms of base shear versus top displacement.

7

Fig.9a shows the double pushover analysis considering earthquake damage state D_I for positive (right) and negative (left) tsunami directions. The earthquake loading-unloading is shown by a black continuous line, following the color convention considered in Fig.4. The behavior observed in Fig.9a for damage state D_I is very similar to the one depicted in Fig.8a for the case D_0. In fact, peak base shear and top displacements are very similar between cases D_0 and D_I, with an average difference (i.e. considering both directions and both Froude numbers) of 0.86% and 2.45%, respectively. Neither previous damage nor tsunami direction have significant influence on the results when previous earthquake damage D_I is considered.

Similarly, Fig.9b shows the double pushover analysis results for the earthquake at damage state D_{II} for both tsunami directions. In this case, the earthquake pushover reaches a higher base shear and higher top displacement than in the case of damage state D_I. The curve shape, peak base shear and top displacement are again very similar to cases D_0 and D_I. The same observations can be derived from Fig.9c regarding damage state D_{III} , i.e., the influence of the Froude number is significant in terms of the expected behavior and peak values, but previous earthquake damage has almost no influence on the response.

Finally, Fig. 9d shows the results for the case with previous earthquake damage D_{IV}. In this case, the earthquake unloading produces a condition of significant residual displacement where the tsunami loading starts. As a consequence, base shear is reduced for both Froude numbers, with respect to the other damage states. Additionally, the positive tsunami loading is the worst-case scenario where lower base shear is reached for both Froude numbers. Also, higher top displacement is observed in the positive tsunami respect to the other damage states (Fig. 9d). This is explained fundamentally by the significant initial displacement and the reduction in stiffness due to the failure located at the critical section after the earthquake for damage state D_{IV}.

Fig.10 shows the crack pattern at the maximum capacity of the structure under a tsunami pushover for the case with no previous damage D_0. Maximum crack strains are located in the first basements of wall 2, as bounded in Fig.10. Normal crack strains with a 45° angle are observed. It is to be noted that even though wall 1 presents more cracks, the magnitude of the strains is significantly higher on wall 2.
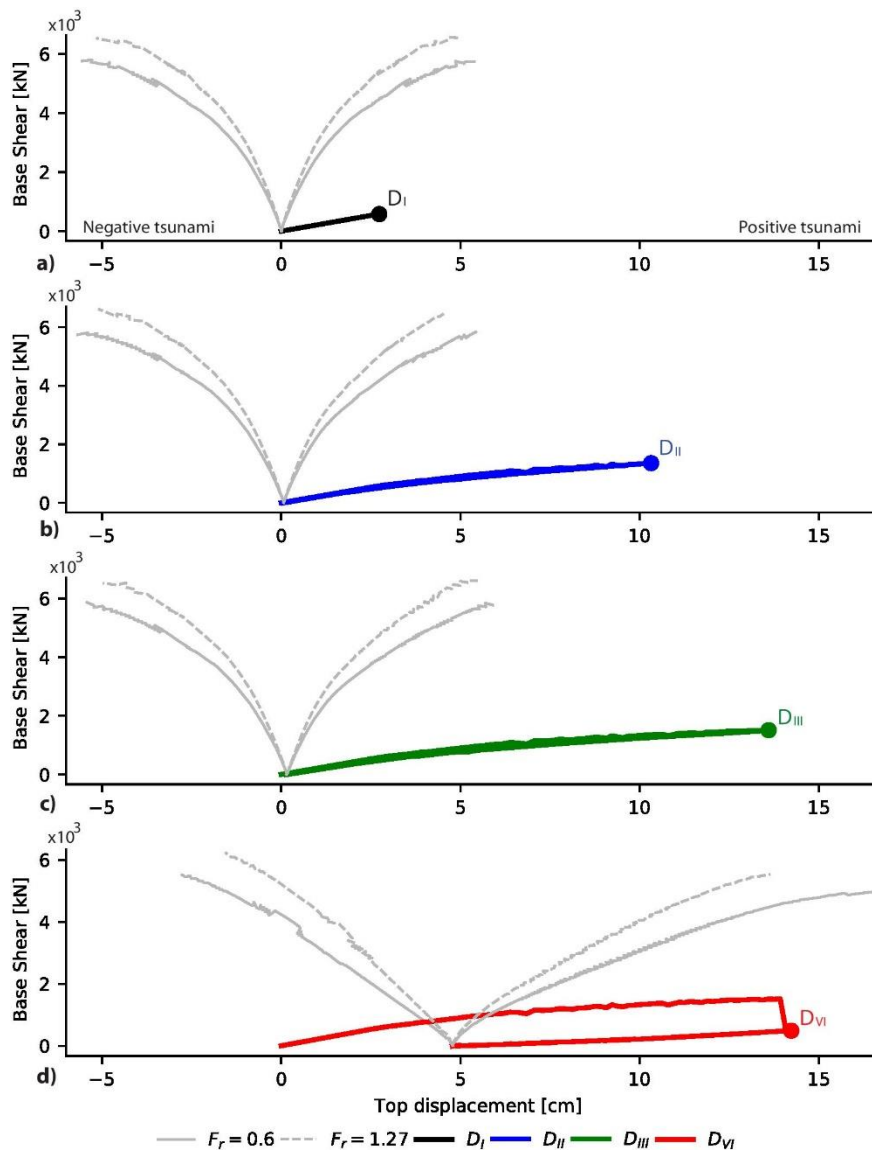
Fig. 9 – Earthquake and tsunami in sequence on simplified model for F_r=0.6 and F_r=1.27: a) tsunami from D_I; c) tsunami from D_{II}; d) tsunami from D_{III}; e) tsunami from D_{IV}

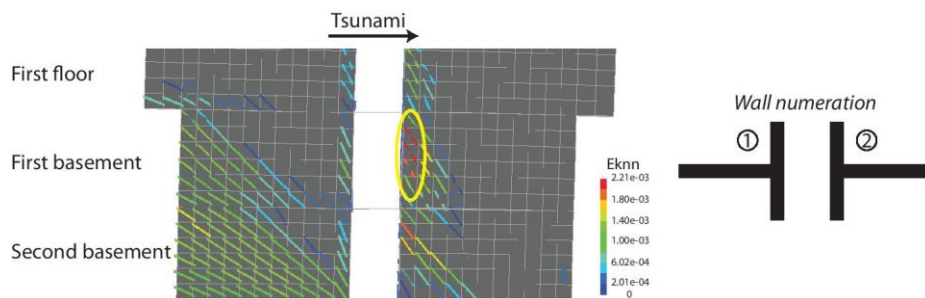Fig. 10 – Normal crack strains (Eknn) at maximum capacity for tsunami without previous earthquake damage D_0 and F_r=0.6

9

Fig.11a shows the crack pattern for earthquake damage state D_{III}, while Fig.11b and 11c show the crack pattern at peak of the negative and positive sequential tsunami after earthquake damage D_{III}, respectively. For earthquake damage state D_{III} (Fig.11a), maximum crack strains are observed in wall 1 on the first floor (bounded in Fig.11a). In the case of negative tsunami (Fig.11b), maximum crack strains are located in the first basement of wall 1, in an area where little damage is observed from the earthquake (Fig.11a). In the case of a positive tsunami (Fig.11c), maximum crack strains are now located in the first basement of wall 2. Thus, the areas with higher damage due to the tsunami (positive or negative) are different than the areas damaged by the earthquake. Additionally, the magnitude and location of cracks caused by a negative or positive tsunami starting from damage state D_{III} (Fig.11b and 11c) are very similar to the ones obtained in the case without previous earthquake D_0, as shown in Fig.10. This supports the conclusion that the previous earthquake damage has no significant influence on tsunami behavior for damage states D_I, D_{II} and D_{III}.
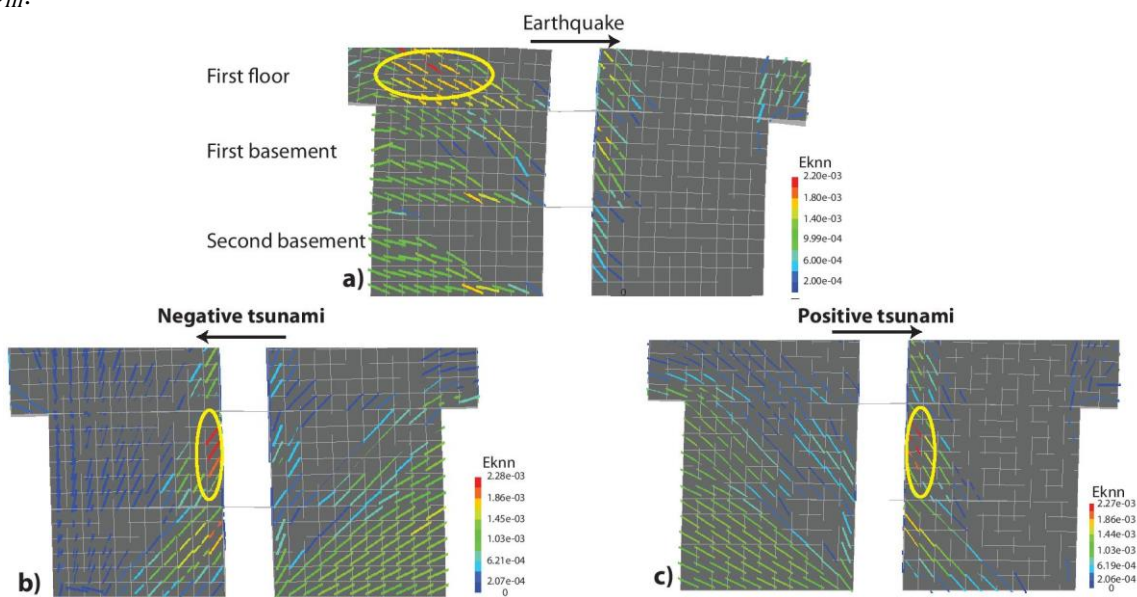

Fig. 11 – Normal crack strains (Eknn): a) damage state D_{III} due to earthquake pushover; b) maximum capacity under negative tsunami after earthquake pushover with D_{III}; and c) maximum capacity under positive tsunami after earthquake pushover with D_{III}

Similar to Fig.11, Fig.12 illustrates the crack pattern for the earthquake damage state D_{IV} (Fig.12a), the peak of negative tsunami (Fig.12b), and peak of positive tsunami (Fig.12c). Maximum crack strains at damage state D_{IV} (Fig.12a) are nearly 3.8 times the maximum crack strains observed in the case with earthquake damage state D_{III} (Fig.11a) and are concentrated at the critical section of wall 2, i.e., just below the setback. In the case of negative tsunami (Fig.12b), although maximum crack strains are concentrated in the critical section of wall 2, their magnitude is lower, because the tsunami is applied in the opposite direction to the earthquake. The new cracks with higher magnitude are now located at the bottom of wall 2, in a zone that was not previously damaged by the earthquake. In the case of positive tsunami (Fig.12c), maximum crack strains are located at the critical section of wall 2, i.e., the same section were earthquake damage was concentrated (Fig.12a). Thus, the structure with damage state D_{IV} followed by a positive tsunami will present a concentration of cracks located in the same area previously damaged by the earthquake. This is consistent with the previous observation that positive tsunami loading is the worst-case scenario, for both Froude numbers. Based on this, the tsunami loading direction only demonstrates different behavior for an earthquake
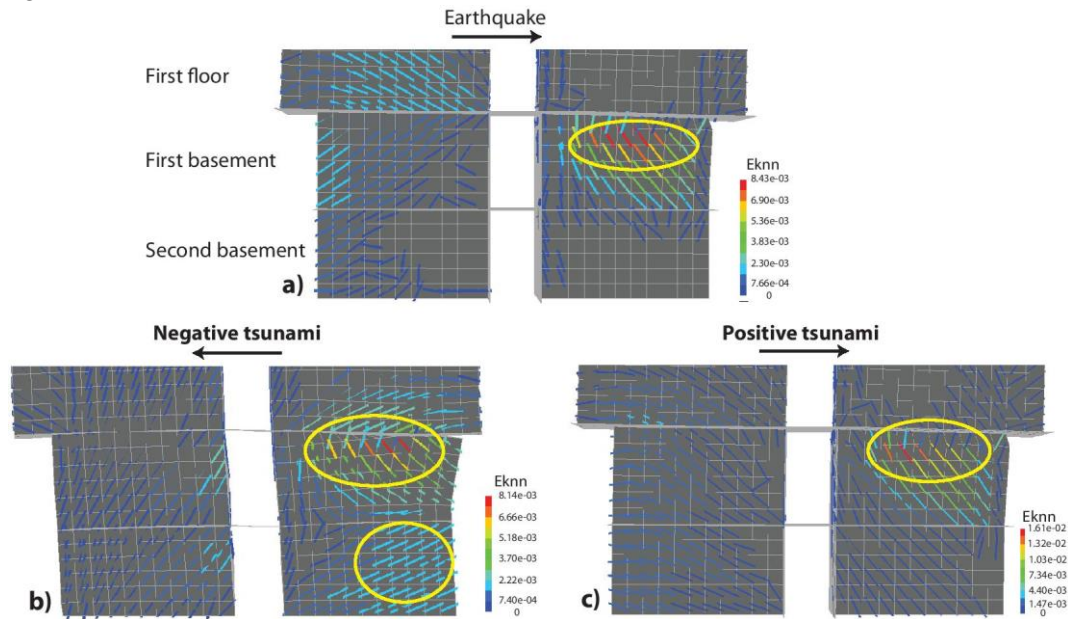
10

with damage state D_{IV}.

Fig. 12 – Normal crack strains (Eknn): damage state D_{IV} due to earthquake pushover; b) maximum capacity under negative tsunami after earthquake pushover with D_{IV}; and c) maximum capacity under positive tsunami after earthquake pushover with D_{IV}

6. Conclusions

This paper investigated the behavior of a typical RC wall Chilean building subjected to the sequential action of earthquake and tsunami. The software DIANA [10] was used to perform inelastic finite element models of a damaged wall of the case-study building.

A double pushover analysis considering earthquake and tsunami in sequence was performed to a simplified model of the building, based on a representative fictitious slice. The earthquake pushover was conducted first until a specific damage level was reached, ranging from damage level I to IV. Then, the earthquake was unloaded until zero base shear; finally, the tsunami loads were applied on the damaged structure. Two different Froude numbers and two tsunami directions were considered. Results consistently showed the tsunami response of the structure to be very sensitive to the Froude number (F_r).

Additionally, results show that the tsunami capacity of the structure was not significantly affected by the previous earthquake damage for damage states D_I, D_{II} and D_{III}. For these cases, the maximum base shear and peak displacement were independent of the previous earthquake damage, and rather independent of the tsunami direction as well. The results were also very similar to the case without previous damage. However, when the earthquake damage state D_{IV} was considered, the tsunami capacity was reduced, and the tsunami direction also had a significant effect. In particular, a positive tsunami load applied to a damage state D_{IV} turned out to be the most critical case. In such case, the tsunami load increased the crack strains in an area previously damaged by the earthquake, so lower tsunami heights were achieved for both Froude numbers.

7. Acknowledgements

8. References

[1] World Bank (2005): Indonesia: Preliminary Damage and Loss Assessment. Washington. USA.

[2] Kajitani Y, Chang S, Tatano H (2013): Economic Impacts of the 2011 Tohoku-Oki Earthquake and Tsunami. *Earthquake Spectra*, **29** (S1), S457-S478.

[3] Palermo D, Nistor I, Saatcioglu M, Ghobarah A (2013): Impact and damage to structures during the 27 february 2010 Chile tsunami 1. *Canadian Journal of Civil Engineering*, **40**, 750-758.

[4] De la Llera J, Rivera F, Mitrani-Reiser J, Jünemann R, Fortuno C, Ríos M, et al (2017): Data collection after the 2010 Maule earthquake in Chile. *Bulletin of Earthquake Engineering*, **15**, 555-588.

[5] Petrone C, Rossetto T, Baiguera M, De la Barra C, Ioannou I (2020): Fragility functions for a reinforced concrete structure subjected to earthquake and tsunami in sequence. *Engineering Structures*, **205**, 110120.

[6] De la Barra C (2017): A Double Pushover Approach for the Assessment of a Chilean Reinforced Concrete Shear Wall Building Subjected to Earthquake and Tsunami in Sequence. *Master's thesis*, University College, London, England.

[7] Latcharote P (2015): Development of Nonlinear Analysis Method to Simulate Nonlinear Behavior of RC Walls in RC Wall-Frame Buildings Suffering Damage from Earthquake and Subsequent Tsunami. *Ph.D. thesis*, Kochi University of Technology, Kami, Japan.

[8] Jünemann R, De la Llera JC, Hube MA, Vásquez JA, Chacón M (2016): Study of the damage of reinforced concrete shear walls during the 2010 Chile earthquake: Study of Damage of RC Shear Walls during the 2010 Chile Earthquake. *Earthquake Engineering & Structural Dynamics,* **45** (10), 1621-1641.

[9] Vásquez JA, Jünemann R, De la Llera JC, Hube MA (2018): Three-dimensional nonlinear response history analyses for earthquake damage assessment: a case study RC wall building. *Earthquake Spectra*, Unpublished results.

[10] DIANA FEA (2007): User's Manual. URL: https://dianafea.com/manuals/d102/Diana.html.

[11] Dashti F, Dhakal R, Pampanin S (2017): Numerical Modeling of Rectangular Reinforced Concrete Structural Walls. *Journal of Structural Engineering*, **143** (6), 04017031.

[12] Vecchio F, Collins M (1986): The Modified Compression-Field Theory for Reinforced Concrete Elements Subjected to Shear. *Journal Proceedings*, **83**, 219-231.

[13] Hordijk DA (1991): Local approach to fatigue of concrete, *Ph.D. thesis*, Universitei Delft, Delft, The Netherlands.

[14] Menegotto M, Pinto PE (1973): Method of analysis of cyclically loaded RC plane frames including changes in geometry and non-elastic behavior of elements under normal force and bending. *Preliminary Report IABSE*, Lisbon, Portugal.

[15] DIANA FEA (2012): Q20SH URL: https://dianafea.com/manuals/d944/ElmLib/node286.html.

[16] Tagle SJ, Jünemann R, Vásquez JA, de la Llera JC, Baiguera M (2019): Performance of a Reinforced Concrete (RC) Wall Building Subjected to Sequential Earthquake and Tsunami Loading. *Engineering Structures*, Under review.

[17] Qi ZX, Eames I, Johnson ER (2014) : Force acting on a square cylinder fixed in a free-surface channel flow. *Journal of Fluid Mechanics*, **756**, 716-727.

[18] Asai T, Nakano Y, Tateno T, Fukuyama H, Fujima K, Sugano T, et al (2012): Tsunami Load Evaluation Based on Field Investigations of the 2011 Great East Japan Earthquake. *15 WCEE*, Lisbon, Portugal.